Monthly Notices
of the
ROYAL ASTRONOMICAL SOCIETY

Mon. Not. R. Astron. Soc. **402,** 1995–2008 (2010) doi:10.1111/j.1365-2966.2009.16031.x

Luminosity function and radial distribution of Milky Way satellites in a ΛCDM Universe

Andrea V. Macciò,[1⋆] Xi Kang,[1] Fabio Fontanot,[1] Rachel S. Somerville[1,2] Sergey Koposov[1,3,4] and Pierluigi Monaco[5,6]

[1]*Max-Planck-Institut für Astronomie, Königstuhl 17, 69117 Heidelberg, Germany*
[2]*Space Telescope Science Institute, 3700 San Martin Drive, Baltimore, MD 21218, USA*
[3]*Institute of Astronomy, University of Cambridge, Madingley Road, Cambridge*
[4]*Sternberg Astronomical Institute, Universitetskiy pr. 13, 119992 Moscow, Russia*
[5]*Dipartimento di Astronomia, Università di Trieste, via Tiepolo 11, 34131 Trieste, Italy*
[6]*INAF-Osservatorio Astronomico, Via Tiepolo 11, I-34131 Trieste, Italy*

Accepted 2009 November 11. Received 2009 October 12; in original form 2009 March 25

ABSTRACT

We study the luminosity function (LF) and the radial distribution of satellite galaxies within Milky Way (MW) sized haloes as predicted in cold dark matter based models of galaxy formation, making use of numerical *N*-body techniques as well as three different semi-analytic models (SAMs) galaxy formation codes. We extract merger trees from very high-resolution dissipationless simulations of four Galaxy-sized DM haloes, and use these as common input for the SAMs. We present a detailed comparison of our predictions with the observational data recently obtained on the MW satellite LF. We find that SAMs with rather standard astrophysical ingredients are able to reproduce the observed LF over six orders of magnitude in luminosity, down to magnitudes as faint as $M_V = -2$. We also perform a comparison with the actual observed number of satellites as a function of luminosity, by applying the selection criteria of the SDSS survey to our simulations instead of correcting the observations for incompleteness. Using this approach, we again find good agreement for both the luminosity and radial distributions of MW satellites. We investigate which physical processes in our models are responsible for shaping the predicted satellite LF, and find that tidal destruction, suppression of gas infall by a photoionizing background, and supernova feedback all make important contributions. We conclude that the number and luminosity of MW satellites can be naturally accounted for within the (Λ)cold dark matter paradigm, and this should no longer be considered a problem.

Key words: gravitation – methods: *N*-body simulation – methods: numerical – galaxies: haloes – cosmology: theory – dark matter.

1 INTRODUCTION

The Milky Way (MW) environment provides an excellent laboratory for astrophysics. It has been used extensively in the past decades to test theoretical models of galaxy formation. In particular, the number density of satellites around our Galaxy has long been considered one of the major problems for the otherwise quite successful Λ cold dark matter (ΛCDM) paradigm.

About a decade ago, *N*-body simulations attained sufficient dynamic range to reveal that in CDM models, all haloes should contain a large number of embedded subhaloes that survive the collapse and virialization of the parent structure (Klypin et al. 1999; Moore et al. 1999; and more recently Diemand, Kuhlen & Madau 2007). Although the predicted number of substructures was in reasonable agreement with observed luminosity functions (LFs) in cluster sized haloes, in MW sized haloes the number of predicted subhaloes exceeded the number of observed satellites by at least an order of magnitude: the known satellite population at that time consisted of about 40 satellites with $V_c \gtrsim 20\,\mathrm{km\,s^{-1}}$ in the Local Group (e.g. Mateo 1998), while the simulations predicted about 300 subhaloes with $V_c \gtrsim 20\,\mathrm{km\,s^{-1}}$ (Klypin et al. 1999; Moore et al. 1999).

Several astrophysical solutions to this problem have been proposed. Many authors have pointed out that accretion of gas into low-mass haloes and subsequent star formation is inefficient in the presence of a strong photoionizing background, as this

⋆E-mail: maccio@mpia.de

© 2009 The Authors. Journal compilation © 2009 RAS

background radiation raises the entropy of the gas, preventing it from accreting on to small dark matter haloes and lengthening the cooling time of that gas which has accreted (e.g. Babul & Rees 1992; Efstathiou 1992; Quinn, Katz & Efstathiou 1996; Thoul & Weinberg 1996). Several studies showed quantitatively that this suppression of gas infall by cosmic reionization could plausibly reconcile the observed and predicted numbers of 'classical' Local Group satellites (Bullock, Kravtsov & Weinberg 2000; Benson et al. 2002; Somerville 2002; Ricotti, Gnedin & Shull 2002; Read, Pontzen & Viel 2006). It was also pointed out that tidal stripping and heating as satellites orbited in the potential of the larger galaxy could cause dramatic mass loss, even decreasing the circular velocity in the inner parts of the subhalo (Kravtsov, Gnedin & Klypin 2004; Taylor & Babul 2004; Zentner et al. 2005). Thus, many Local Group satellites may inhabit dark matter (sub-)haloes that are much less massive than they were at the time that they were accreted by their host halo.

In recent years, the Sloan Digital Sky Survey (SDSS; Adelman-McCarthy et al. 2008) has changed our view of the MW and its environment. The SDSS has made it possible to carry out a systematic survey for satellite galaxies, which are detectable through their resolved stellar populations down to extremely low surface brightness. As a result the number of known dwarf spheroidals has doubled in the recent past (e.g. Willman et al. 2005; Zucker et al. 2006; Belokurov et al. 2007; Gilmore et al. 2007; Irwin et al. 2007). Spectroscopic surveys subsequently measured the velocity dispersions of these systems, and confirmed their galactic nature (Martin et al. 2007; Simon & Geha 2007). This recently discovered population of ultra faint satellites has posed new challenges for models of galaxy formation and opened the possibility to test the ΛCDM paradigm at very small mass scales (e.g. Strigari et al. 2008; Macciò, Kang & Moore 2009).

These new observations have made it possible to probe the faint end of the LF of MW satellites, down to luminosities as faint as 100 $L_\odot$. Moreover, the homogeneous sky coverage of the SDSS enables a robust determination of the detection limits for faint satellites. Koposov et al. (2008, hereafter SK08) provided the first determination of the volume corrected MW satellite LF down to these extremely faint limits, by assuming various simple radial distribution functions for the satellite population and applying the SDSS detection limits.

In light of the discovery of the new ultra-faint dwarf population and the improvements in the numerical modelling of galaxy formation, it is now timely to revisit the issue of whether the basic properties of satellite galaxies around the MW, such as their number density, radial distribution, and mass-to-light ratios, can be reproduced within current cosmological ΛCDM-based models. It is also interesting to ask what physical processes might plausibly give rise to this population of extremely low-luminosity galaxies.

In this paper, we combine merger trees extracted from very high resolution *N*-body simulations with three different semi-analytic model (SAM) codes. These merger trees describe the hierarchical assembly of a MW-like halo, while the SAMs are used to predict the relationship between the dark matter (sub)haloes and observable galaxy properties, allowing us to make a direct and detailed comparison with observational data.

The goal of this work is not only to test whether the observed properties of MW satellites, including the recently discovered faint population, can be reproduced within the ΛCDM model, but also to understand how and when this extreme population formed. We aim to understand how various mechanisms [such as supernova (SN) feedback, cosmic photoionization and tidal stripping] may shape the luminosities of galaxies populating low-mass dark matter substructures orbiting around MW-like galaxies.

Table 1. Dark matter halo parameters.

Halo	Mass ($10^{12}\,h^{-1}\,M_\odot$)	$N_{\rm part}$ (10^6)	$R_{\rm vir}$ (kpc h^{-1})	$V_{\rm circ}$ (km s^{-1})
G0	0.88	2.12	197	178
G1	1.22	2.93	219	188
G2	1.30	3.12	250	203
G3	2.63	5.64	268	236
$G1_{HR}$	1.15	31.5	211	184

The remainder of this paper is organized as follows. In Section 2, we describe the numerical simulations. In Section 3, we briefly summarize the SAMs used in our study, highlighting the differences among the models. Section 4 contains a detailed description of the observational data used in this work. In Section 5, we compare the LF, and radial distribution of simulated satellites with observational data. Finally, in Section 6, we present our main conclusions.

2 SIMULATIONS

The *N*-body simulations of this study were obtained using PKDGRAV, a tree code written by Joachim Stadel and Thomas Quinn (Stadel 2001). The initial conditions are generated with the GRAFIC2 package (Bertschinger 2001). The starting redshift z_i is set to the time when the standard deviation of the smallest density fluctuations resolved within the simulation box reaches 0.2 (the smallest scale resolved within the initial conditions is defined as twice the intra-particle distance). The cosmological parameters are chosen to be: $\Omega_\Lambda = 0.732$, $\Omega_{\rm m} = 0.268$, $\Omega_{\rm b} = 0.044$, $h = 0.71$ and $\sigma_8 = 0.9$, and are in reasonable agreement with the recent *Wilkinson Microwave Anisotropy Probe (WMAP)* mission results (Komatsu et al. 2009).

We selected four candidate haloes with a mass similar to the mass of our Galaxy ($M \sim 10^{12}\,M_\odot$) from an existing low resolution dark matter simulation (300^3 particles within 90 Mpc) and resimulated them at higher resolution. Our high resolution haloes all have a quiet merging history with no major merger after $z = 2$, and thus are likely to host a disc galaxy at the present time (with the exception of G3, which we discuss further below). The standard high-resolution runs are 12^3 times more resolved in mass than the initial simulation: the dark matter particle mass is $m_{\rm d} = 4.16 \times 10^5\,h^{-1}\,M_\odot$, where each dark matter particle has a spline gravitational softening of $355\,h^{-1}$ pc. Some of the main properties of the resimulated haloes are listed in Table 1. One of the haloes, namely G3, has a mass greater than the expected mass of the MW and has experienced a major merger at $z = 1.5$ so it is likely to host an elliptical galaxy. In order to check possible resolution effects (especially in the construction of the merger tree) we resimulated one of the haloes (namely G1) with higher resolution (27^3 times with respect to the low resolution), with more than 32 million particles within the virial radius ($G1_{HR}$ in Table 1), reaching a dark matter particle mass of $m = 3.65 \times 10^4\,h^{-1}\,M_\odot$.

For the purpose of constructing accurate merger trees for each simulated halo, we analyse 53 output times between $z = 20$ and 0. For each snapshot, we look for all the virialized isolated haloes within the high-resolution region using a Spherical Overdensity (SO) algorithm. We use a time varying virial density contrast determined using the fitting formula presented in Mainini et al. (2003). We include in the halo catalogue all the haloes with more than 100 particles (see Macciò et al. 2007; Macciò, Dutton & van den Bosch

2008 for further details on our halo finding algorithm). Our procedure to construct merger trees is described in detail in Macciò et al. (2009). We used all particles within 1.5 times the virial radius of a given 'root' halo at $z = 0$ and then track them back to the previous output time. We then make a list of all haloes at that earlier output time containing marked particles, recording the number of marked particles contained in each one. We use the two criteria suggested in Wechsler et al. (2002) for halo 1 at one output time to be labelled a 'progenitor' of halo 2 at the subsequent output time. In our language, halo 2 will then be labelled as a 'descendant' of halo 1 if (i) more than 50 per cent of the particles in halo 1 end up in halo 2 or if (ii) more than 75 per cent of halo 1 particles that end up in any halo at time-step 2 end up in halo 2 (this second criterion is mainly relevant during major mergers). Thus, a halo can have only one descendant but there is no limit to the number of progenitors. On an average, there are 20 000 progenitors for haloes G0-G3, while the number of progenitors for the $G1_{HR}$ run is close to 100 000.

In order to identify subhaloes in our simulation, we have run the parallel hybrid halo finder AHF (AMIGA halo finder, which can be downloaded freely from http://popia.ft.uam.es/AMIGA) described in detail in Knollmann & Knebe (2009). AHF locates local overdensities in an adaptively smoothed density field as prospective halo centres. The local potential minima are computed for each of these density peaks and the gravitationally bound particles are determined. Only peaks with at least 50 bound particles are considered as haloes and retained for further analysis. As subhaloes are embedded within their respective host halo, their own density profile usually shows a characteristic upturn at a radius $r_t \lesssim r_{vir}$, where r_{vir} would be their actual (virial) radius if they were found in isolation. We use this 'truncation radius' r_t as the outer edge of the subhaloes and hence (sub-)halo properties (i.e. mass) are calculated using the gravitationally bound particles inside r_t.

3 SEMI-ANALYTIC MODELS

We make use of three different SAM codes in order to predict the observable properties of galaxies that inhabit the dark matter haloes and subhaloes identified in the *N*-body simulations described above (see Baugh 2006 for a recent review on the semi-analytic approach). We will consider predictions from the most recent implementations of three different SAMs, developed independently by different groups: (i) the Kang et al. (2005) model that has been recently updated in Kang (2009, hereafter K09); (ii) the fiducial model of Somerville et al. (2008, hereafter S08), which builds on the original formulation presented in Somerville & Primack (1999) and Somerville, Primack & Faber (2001); (iii) MORGANA, first presented in Monaco, Fontanot & Taffoni (2007) and then updated in Lo Faro et al. (2009). Since all SAMs assume that DM haloes are the sites where galaxy formation takes place and they need a proper description of their assembly history, we will use the four merger trees extracted from *N*-body simulations of the G0–G3 haloes (see Section 2) as a common input. In order to increase the statistical robustness of our results, in Section 5.2 we also consider a larger set of realizations of merger trees obtained using the extended Press–Schechter (EPS) formalism (e.g. Somerville & Kolatt 1999; Parkinson, Cole & Helly 2008) for K09 and S08 and the Lagrangian code PINOCCHIO (Monaco, Theuns & Taffoni 2002) for MORGANA.

All the SAMs considered in this work parametrize in different ways the main physical processes acting on the baryonic component, such as atomic cooling, cosmic reionization, star formation, SNe feedback, metal production and dust attenuation. For the sake of simplicity, we will discuss here only those processes relevant in shaping the LF of MW satellites. We refer the reader to the original works for a more detailed discussion on the modelling of physical processes (see also Fontanot et al. 2009, for a comparison between different SAMs).

Although our simulations resolve subhaloes,[1] we do not record the fate of subhaloes in our merger trees or make use of this information in the SAMs. When a subhalo is accreted, its position is initially either set equal to the virial radius of the parent halo at that time (K09 and S08) or extracted from a suitable distribution of radial distances (MORGANA). Moreover, the orbital parameters (velocity and orbit eccentricity) for each infalling satellite are randomly selected from a distribution motivated by the statistics of satellite orbits in cosmological simulations. The dynamical evolution (and so the survival probability) of each subhalo is then computed by estimating the time required for the subhalo to lose all of its orbital energy due to dynamical friction against the background DM potential (using updated variants of the classical Chandrasekhar formula).

Each of the models that we have considered applies a different set of criteria to determine when satellites are destroyed by tidal stripping. In the K09 models, a subhalo is considered to be tidally destroyed if either it loses more than 98 per cent of its mass (e.g. Peñarrubia, McConnachie & Navarro 2008) or its mass falls below $6.5 \times 10^6\,M_\odot$, which is the minimum mass observed for MW satellites (Strigari et al. 2008). In the S08 model, satellites are considered to be tidally destroyed when their stripped mass drops below the mass contained within a fixed fraction of the halo's original NFW (Navarro, Frenk & White 1997) scale radius r_s (following Zentner & Bullock 2003; Taylor & Babul 2004). In MORGANA, the tidal radius is computed at the first periastron of the satellite orbit by computing the radius at which the density of the unperturbed satellite is equal to the density of the main DM halo at the periastron. All the mass (whether dark, stellar or gaseous) external to the tidal radius (i.e. at a lower density) is then considered unbound. The MORGANA estimates of the radii of the bulge and disc components, plus assumed density profiles for the stars and gas, are used to estimate the fraction of the baryonic mass that lies outside the tidal radius.

In all three models, the effect of reionization is expressed in terms of a 'filtering mass' (e.g. Gnedin 2000). This filtering mass corresponds to the mass at which haloes will only be able to accrete half of the universal baryonic content. The fraction of baryons that can be accreted as hot gas is parametrized using the following expression (Gnedin 2000):

$$f_{b,acc}(z, M_{vir}) = \frac{f_b}{[1 + 0.26 M_F(z)/M_{vir}]^3}\,, \quad (1)$$

where f_b is the universal baryon fraction and M_{vir} is the halo virial mass. The filtering mass as a function of redshift $M_F(z)$ depends on the reionization history of the Universe, and is parametrized using the fitting formulae provided by Kravtsov et al. (2004, but see Section 5.4.1).

Massive stars and SNe may impart thermal and kinetic energy to the cold interstellar medium: in the K09 and S08 models, the rate of reheating of cold gas due to SN feedback is given by an expression of the form:

$$\dot{m}_{rh} = \epsilon_0^{SN} \left(\frac{V_{disc}}{V_0}\right)^{\alpha_{rh}} \dot{m}_* \quad (2)$$

[1] From this point on, we refer to the DM haloes living within the virial radius of larger haloes as 'substructure' or 'subhaloes', while we refer to the all the galaxies except the central galaxy of the larger halo as 'satellites'.

© 2009 The Authors. Journal compilation © 2009 RAS, MNRAS **402,** 1995–2008

where $\epsilon_0^{\rm SN}$ and $\alpha_{\rm rh}$ are free parameters and $\dot{m}_*$ is the star formation rate. K09 and S08 adopt similar values of $\epsilon_0^{\rm SN}$ and $\alpha_{\rm rh} \sim -2$, chosen to reproduce the faint-end slope of the observed $z = 0$ global galaxy LF or the low-mass end of the stellar mass function. In contrast, the MORGANA model adopts a recipe based on the notion of a self-regulated feedback loop between star formation and SNe (Monaco 2004), which roughly corresponds to $\epsilon_0^{\rm SN} = 1$ and $\alpha_{\rm rh} = 0$ in terms of equation (2). However, we find that in order to reproduce the MW satellite LF with MORGANA we need to introduce a strong dependence of the mass loading factor $\eta \equiv \dot{m}_{\rm rh}/\dot{m}_*$ on the galaxy circular velocity[2] ($\alpha_{\rm rh} = -4$). This suggests that the phenomenological scaling in equation (2) is a key to the success of galaxy formation models in the ΛCDM context in predicting the MW satellite LF.

It is worth noting that the ingredients of these SAMs have all been developed with much larger galaxies in mind, and the models have previously been calibrated mainly against observations of relatively luminous galaxies ($M_* \gtrsim 10^9\,{\rm M}_\odot$ or $M_V \lesssim -16$). It is quite unclear whether the standard semi-analytic empirical recipes for e.g. star formation or SN feedback should apply in galaxies as tiny as the ultra-faint MW dwarfs, which may form out of just a few molecular clouds. Therefore, it is quite an interesting experiment to see how well these models perform when extended to these very different mass scales.

4 OBSERVATIONAL DATA

We test our MW models against observations by focusing on two key aspects of MW satellite galaxy properties: their luminosity and radial distributions.

For the LF, we use the results of SK08. SK08 recently presented a quantitative search methodology for MW satellites in the SDSS DR5 data and used this method to compute detection efficiency maps, which ultimately allowed the construction of the first completeness-corrected satellite galaxy LF (see also Walsh, Willman & Jerjen 2009). SK08 measured the LF down to $M_V = -2$, and found that it can be described by a single power law of the form ${\rm d}N/{\rm d}M_v = 10 \times 10^{0.1(M_V+5)}$. At the very faint end ($M_V > -5$), in order to compute the completeness correction, a radial satellite distribution around the host must be assumed; in all the LF plots presented in this paper the upper data points (always shown as open circles with no error bars) are obtained assuming an isothermal density distribution while the lower points (solid circles with error bars) are obtained assuming an NFW (Navarro et al. 1997) distribution.

We also use a reverse approach to addressing the completeness issue by performing the comparison in 'observational space'. Instead of assuming a radial distribution for the observed galaxies, we apply the detection criteria of the SDSS to our simulations (see Section 5.3 for more details) and compare directly with the raw data from the SDSS. For this comparison, we construct a 'hybrid' data set. For satellites brighter than $M_V = -9$, in order to increase the number statistics, we gather together satellites from the MW and the Andromeda galaxy (data from Mateo 1998; Metz, Kroupa & Jerjen 2007), and we assign a weight of $w = 0.5$ to each satellite, assuming that current surveys are complete down to this limit. For fainter satellites, we collect data from (Martin, de Jong & Rix 2008, hereafter MdJR08) and, in order to account for the fact that the SDSS surveyed only one-fifth of the sky, we set $w = 5$ for these faint galaxies. The adopted M_V threshold for splitting the observational sample is justified by the low luminosity of all newly discovered satellites both around the MW and the Andromeda galaxy (McConnachie et al. 2008).

In addition, using the same data set described above, we compute the cumulative radial distribution of satellites (i.e. the number of satellites within a given distance from the Sun). Distances for bright satellites are taken from Metz et al. (2007), while we use results compiled in MdJR08 for faint galaxies ($M_V > -9$). In computing the radial distribution, we assign to each galaxy the same weight adopted for the LF.

5 RESULTS

In this section, we present results for both the SAMs and numerical (dissipational and dissipationless) simulations and compare them with the observational data set described in Section 4. First, we compare the dynamical evolution of satellites in SAMs and in N-body simulations, and then we present results for the LF of simulated satellites and analyse the importance of different physical processes (e.g. reionization, stellar stripping and SN feedback) in shaping the LF. We then present results for the radial distribution and compare them with observations.

5.1 Dynamical evolution of subhaloes in SAMs and N-body simulations

In the SAMs investigated here, we chose to make use of N-body based merger trees for 'isolated' (or distinct) haloes only, and to model the dynamical evolution of satellites semi-analytically (see Section 3). Thus, there will not be a one-to-one correspondence between the masses or positions of subhaloes at $z = 0$ in the SAMs and in the actual N-body simulations. In this section, we check that the statistical distributions of subhalo masses and radii predicted by the SAMs are in agreement with those of subhaloes identified in the N-body simulations. This comparison is only possible for the K09 and S08 models, since the MORGANA model does not explicitly follow the dynamics of dark matter substructures. Fig. 1 shows the cumulative subhalo mass function from N-body and SAMs for our four Merger tree G0–G3. The ${\rm G1}_{\rm HR}$ halo is shown for the K09 model only. The SAM results are obtained by averaging over 10 different realizations of the random orbit selection process and are truncated at the N-body mass resolution limit. A simple way to quantify the agreement between two distributions is to perform a Kolmogorov–Smirnov (KS) test (Press et al. 1992). In the following, we will quote as KS results, the probability that two distributions are drawn from the same parent population. K09 and S08 SAMs give an average KS probability of 88 and 90 per cent, respectively, when compared to the subhalo mass function from the N-body simulations, showing thus good agreement with the numerical results.

The radial distribution of satellites is a key piece of information for deciding whether a satellite will be detectable in the SDSS survey. It is therefore important to also check that the SAMs correctly predict the radial distribution of subhaloes within the parent halo. Fig. 2 shows the radial number density of subhaloes (without including the central galaxy); while on average there is a good agreement between SAMs and N-body results for both models (KS test results: 87 and 88 per cent S08 and K09, respectively), there is a systematic off-set between K09 and S08, especially at distances <100 kpc h^{-1}. The reason for this off-set resides in the different fitting formulae for

[2] In order not to spoil the agreement of this model for $M_\star > 10^9\,{\rm M}_\odot$ galaxies, we retain the original recipe $V_c > 100\,{\rm km\,s^{-1}}$ DM haloes and adopt equation (2) in galaxies with $V_c < 100\,{\rm km\,s^{-1}}$.

© 2009 The Authors. Journal compilation © 2009 RAS, MNRAS **402,** 1995–2008

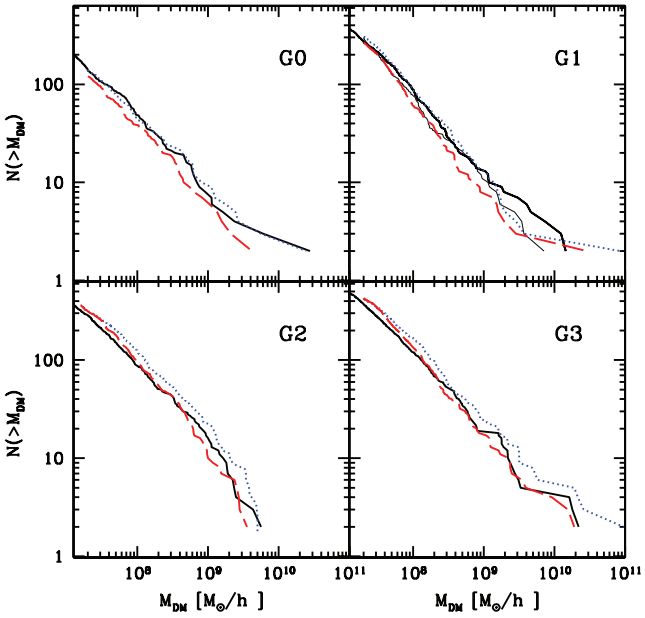

Figure 1. Comparison between the subhalo mass function at $z = 0$ (within $R_{\rm vir}$) in the N-body simulations (solid black line) and the predictions from the SAMs of K09 (red dashed line) and S08 (blue dotted line). Each panel shows results for a different dark matter halo. The (black) thin solid line in the G1 panel shows the results of the K09 SAM when applied to the $G1_{\rm HR}$ halo.

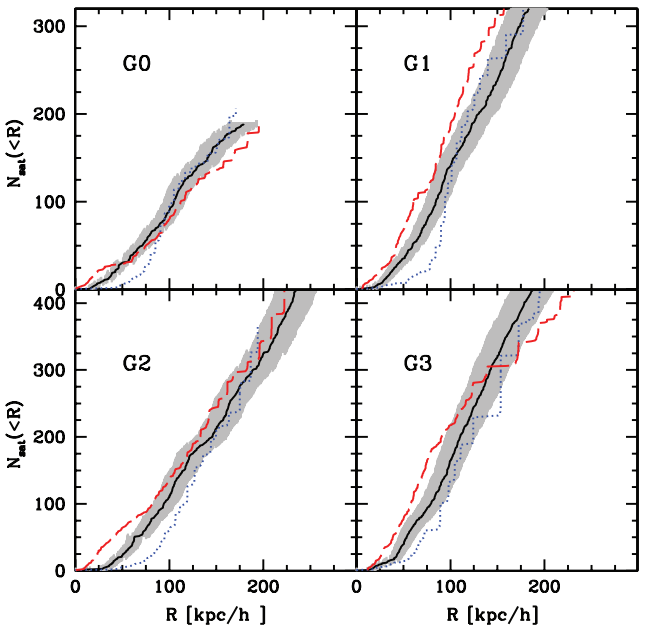

Figure 2. The cumulative number density of satellites as a function of radius from the centre of the parent galaxy. The results from the N-body simulations are shown by the solid (black) line, the shaded (grey) area shows the 1σ scatter over five different realizations of the satellite orbit distribution. Results from the K09 and S08 SAMs are shown by the (red) dashed line and (blue) dotted line, respectively. Each panel shows results for a different dark matter halo.

tidal destruction and dynamical time implemented in the two models, but is nevertheless too small to affect our analysis.

In the SAMs used here, the initial orbit eccentricity of an infalling subhalo is randomly selected from a distribution motivated by the results from cosmological N-body simulations. We checked that the scatter due to different realizations of the orbit distribution is fairly small, and mostly affects the less numerous, massive satellites which are not the focus of our study.

5.2 Satellite luminosity function

We now compute satellite LFs using the four merger trees obtained from the N-body simulations as common input for our SAMs; this allows us to isolate the impact of the different physical ingredients in the SAMs because the DM halo merger histories are exactly the same in all three models. Fig. 3 shows the predictions from our three SAMs, adopting $z_r = 7.5$ as the redshift of reionization. We plot all satellites within $R = 280$ kpc in order to be consistent with the SK08 data set. Solid lines show the mean of satellite distribution and the (grey) shaded area shows the 1σ Poisson scatter around that mean.

All of the models predict that the number of satellites brighter than $M_V = -3$ is of the order of ∼100 and could easily be several hundreds (e.g. G3). This is in agreement with recent estimates of the number of observed satellites obtained by several different approaches (e.g. Madau et al. 2008; Tollerud et al. 2008; Koposov et al. 2009).

All the models show that the total number of satellite galaxies depends on the host halo mass. The LF of the G0 halo (the least massive one, see Table 1) is almost flat and has a lack of satellites at the faint end compared to the MW data. On the other hand, in the most massive halo (G3), the SAMs predict more satellite galaxies at all luminosities than are observed in the MW. This trend between halo mass and the LF does not depend on the SAM used to populate dark matter substructures and indicates that the total mass of the dark matter halo has a quite strong influence in determining the normalization (and shape) of the satellite LF.

All three SAMs considered in this work are able to do a reasonably good job of reproducing the observational data. The K09 and S08 models (upper and middle panels) in Fig. 3 quite successfully reproduce the observed LF for satellite galaxies over the entire luminosity range $-2 \geq M_V \geq -16$. The MORGANA model (lower panels in Fig. 3) tends to predict slightly more satellites at intermediate luminosity ($-10 > M_V > -12$), but it is none the less in good agreement with the observations especially if an NFW distribution is assumed for observed satellites. In the G1 panel for the K09 model, we also show the LF obtained using the $G1_{\rm HR}$ merger tree (dotted black line). We see that the higher resolution merger tree produces almost indistinguishable results.

In some cases, certain models and certain haloes show a dearth or even absence of the most luminous satellites (e.g. S08 and K09 G0, G2 in all models). This should not be a serious cause for concern because the variance in the number of massive subhaloes hosting these luminous satellites is very large and depends on the detailed merger history of the halo. Moreover, the predicted number in the SAM is very sensitive to the random orbit chosen, as discussed in Section 5.1. To assess this issue in a more robust way, we need to increase the number of merger tree realizations of MW mass haloes. We do this by using semi-analytic merger trees instead of the merger trees extracted from N-body simulations. For each model, we generated 40 merger trees for DM haloes in the estimated mass range of the MW dark matter halo, $(0.8–1.2) \times 10^{12}\, h^{-1}\, {\rm M}_\odot$

© 2009 The Authors. Journal compilation © 2009 RAS, MNRAS **402,** 1995–2008

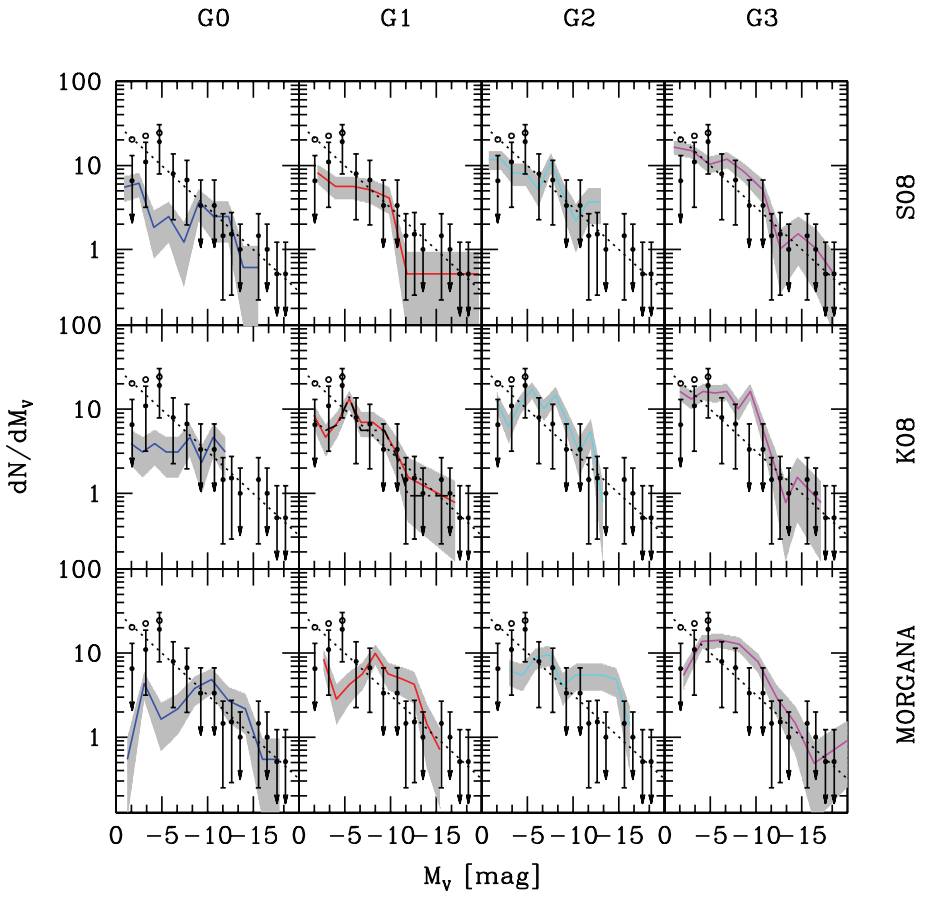

Figure 3. The MW satellite LF predicted by our three SAMs (S08, K09 and MORGANA from top to bottom) using the G0–G3 halo merger trees (from left- to right-hand side), with an assumed reionization redshift $z_r = 7.5$. The median of the satellite distribution is shown by the solid line, while the shaded area represents the 1σ Poisson scatter around the mean. Observational data are taken from SK08 under the assumption of two different radial distributions of satellites, NFW-like (solid circles with error bars) and isothermal (open circles). The arrows on error bars indicate that there is only one galaxy in that particular bin, and so the Poisson error is formally 100 per cent. The dotted line shows a single power-law fitting to the data: $\mathrm{d}N/\mathrm{d}M_v = 10 \times 10^{0.1(M_V+5)}$. In the G1 panel of the K09 model results for the $\mathrm{G1_{HR}}$ run are also shown as a dashed (black) line.

(Klypin, Zhao & Somerville 2002). Each of the SAM codes has its own algorithm for generating merger trees: the K09 and S08 model use different implementation of the EPS algorithm, while MORGANA uses the PINOCCHIO code. Fig. 4 shows the averaged LF for the three SAMs (we tested that the subhalo mass function from the EPS/PINOCCHIO trees is in agreement with the one extracted from the N-body simulations).

The K09 and S08 model are, again, in good agreement with the observational data: they are able to fit the MW LF in the range $-15 < M_V < -2$ (KS test results: 90.9 per cent for S08 and 90.5 per cent for K09). The K09 model shows a small deficit of satellites at brighter magnitudes (especially if compared with S08 and MORGANA) but this occurs where the number of observed satellites has a large error bar due to poor number statistics. Our models produce much better agreement with the number of luminous satellites with $M_V < -15$ relative to the predictions of Benson et al. (2002). Because of the large number of differences between the Benson et al. models and those considered here, we can only speculate on the source of this difference.

It is also interesting to note that the K09 and S08 models suggest that the LF of ultra-faint satellites has a downward kink below about $M_V \sim -6$, in better agreement with the SK08 observational results adopting an NFW, rather than isothermal, radial density distribution for the satellites. An NFW distribution for satellites is predicted by hydrodynamic simulations (Macciò et al. 2006). The comparison between the MORGANA model and the observational results can only be performed down to $M_V = -5$ in this case. This is because the PINOCCHIO code has never been tested on such small scales (e.g. Li et al. 2007) and we did not feel confident in using merger trees with a mass resolution below $\sim 10^8\, h^{-1}\, \mathrm{M}_\odot$. In the tested range for M_V the MORGANA model is also in good agreement with observations (KS test: 90.2 per cent).

In Fig. 5 (lower panel), we plot the stellar mass and luminosity of galactic satellites versus their dark matter subhalo mass; results are shown for the K09 model for all haloes, and are similar for the other models. For this comparison we used both the present dark matter mass [$M_{\rm DM}(z = 0)$] and the mass of the subhalo at the time of accretion [$M_{\rm DM}(z_{\rm acc})$]. The difference between the two reflects the effects of tidal stripping on the dark matter substructure. The correlation between the present-day dark matter mass and luminosity is quite broad and, for low luminosities, $M_{\rm DM}(z = 0)$ at a fixed luminosity spans almost 3 orders of magnitude. This is because tidal stripping of the dark matter subhalo washes out the initial correlation between luminosity and $M_{\rm DM}(z_{\rm acc})$. The same applies to the comparison between the dark and stellar mass of galactic satellites, as shown in the upper panel of Fig. 5.

Recently, Strigari et al. (2008) pointed out that one of the curious properties of the newly discovered population of faint satellites is

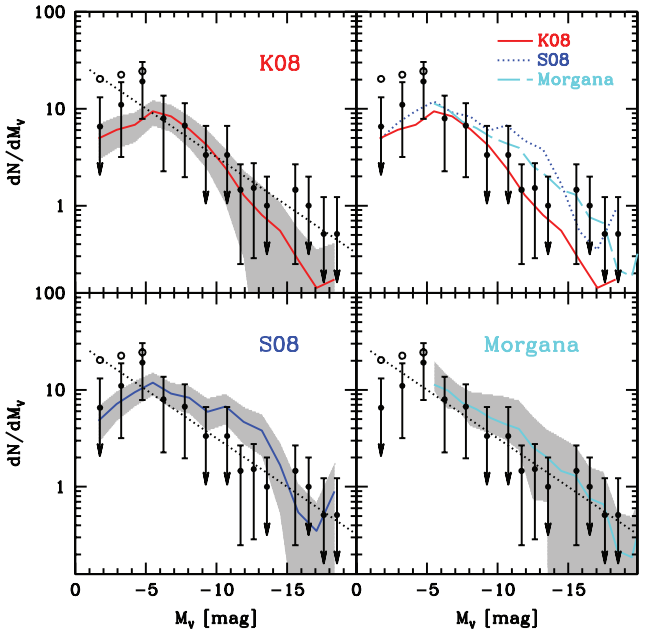

Figure 4. Satellite LF predicted by SAMs using semi-analytic merger trees (EPS and PINOCCHIO, see text for details). Symbols have the same meaning as in Fig. 3. The upper right panel shows the average satellite LF for the three SAMs together. MORGANA results are shown only down to $M_V = -5$, due to a resolution limitation in the PINOCCHIO code; see text for more details.

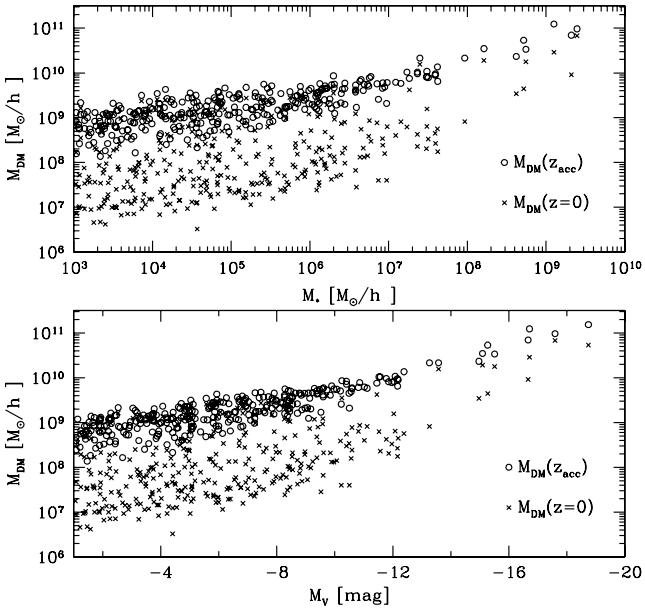

Figure 5. The dark matter mass of galaxy satellites versus their luminosity (lower panel) and stellar mass (upper panel). Open circles show the masses at time of accretion, while crosses show the present (z = 0) dark matter mass. Results are shown for the K09 model for all haloes G0-G3.

that over four orders of magnitude in luminosity, these objects seem to contain a nearly constant total mass within a radius of 300 pc. If we focus on the faint population in Fig. 5, with $-3 < M_V < -10$, we can see that the huge scatter in DM mass at fixed luminosity or stellar mass provides a partial explanation for this apparent 'common' mass scale for the faint satellites. Macciò et al. (2009; see also Li et al. 2009) investigated this in more detail, and presented a direct comparison between the predicted luminosity and the mass within 300 pc for faint satellites in our simulations. They argued that the inner profiles of haloes that are initially very concentrated are less effected by tidal heating than haloes that are less concentrated, so that the mass within 300 pc is reduced for more massive subhaloes (which are less concentrated) relative to less massive ones. When they corrected for this concentration-dependent modification of the inner density profile, they found that the Strigari et al. (2008) results are quantitatively reproduced by our simulations.

5.3 Luminosity function in the observational plane

The LF of SK08 has been determined under certain assumptions for the radial distribution of satellites around our Galaxy. It is also interesting to apply the observational selection criteria to our simulations and compare 'in the observational plane', i.e. with the *raw* data from the SDSS without completeness corrections applied. To make such a comparison, we have applied to our sample of satellites a *visibility* criterion, in order to determine if a given satellite would be detected in the SDSS. We assume that *all* satellites brighter than $M_V = -10$ would be visible and included in the SDSS sample. For fainter satellites, we adopt a criterion based on both satellite distance and luminosity (see SK08 for more details),

$$\log(R/\mathrm{kpc}) < 1.04 - 0.228 \times M_V. \quad (3)$$

In the above formula, the distance R is measured from the Sun and not from the centre of the galaxy. In order to convert our galactocentric distances into helio-centric distances, we assume the Sun to be located at 8 kpc from the centre of the galaxy (8,0,0); moreover, since for each satellite galaxy we only know its distance from the galactic centre, we randomly assign position angles (ϕ, θ) to each of them (see also Tollerud et al. 2008). We exclude from the comparison galaxies more distant than 280 kpc. Moreover since the SDSS covers only approximately one-fifth of the sky we randomly select 1/5 of our satellites. We then average over 100 different realizations of this random sampling. Observational data for the recently discovered SDSS satellites are taken from MdJR08. Fig. 6 shows the comparison between the observations and the LFs obtained with the K09 model (the S08 model gives very similar results and this comparison is not possible for the MORGANA model because it does not provide the distance of satellite galaxies from the main halo). The direct comparison with the observational data confirms our previous results on the LF. Our models are able to reproduce the data for haloes G0–G2, while halo G3 slightly overproduces the number of faint satellites. The agreement between the data and models implies that the distance–luminosity relation of our satellites is similar to the observed one.

The application of the selection criteria of the SDSS to our simulated data also allows us to compare the radial number density of satellites in our models versus observations. Results are shown in Fig. 7. From this figure, we see that our simulations reproduce both the observed slope and normalization of the satellite radial distribution for G0 and G2 (KS test results: 96 and 91 per cent) while the agreement is less good for G1 and G3 (KS: 76 and 77 per cent). The difference for G3 can be ascribed to the overall higher visible satellite number (e.g. Fig. 3). One possible explanation for G1 can be related to its higher formation redshift (half mass in place) than the other two galaxies. This implies that subhaloes will have on average a higher accretion redshift, and thus have more time to sink to the centre.

Finally, in Fig. 8, we compare the radial distribution of DM substructures and 'observable' satellites in the K09 model (obviously, observability depends on many factors, but in this context we

© 2009 The Authors. Journal compilation © 2009 RAS, MNRAS **402,** 1995–2008

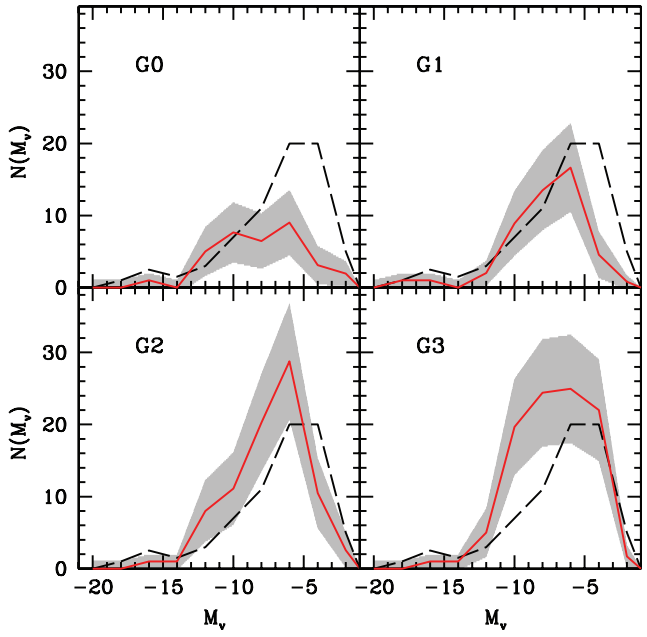

Figure 6. Comparison between the 'raw' SDSS data (uncorrected for completeness) and model predictions with the SDSS visibility criteria applied to the simulations (see text for details). The observational data are shown by the (black) dashed line, the K09 model is shown by the solid (red) line, and the shaded area shows the 1σ Poisson scatter around the mean value.

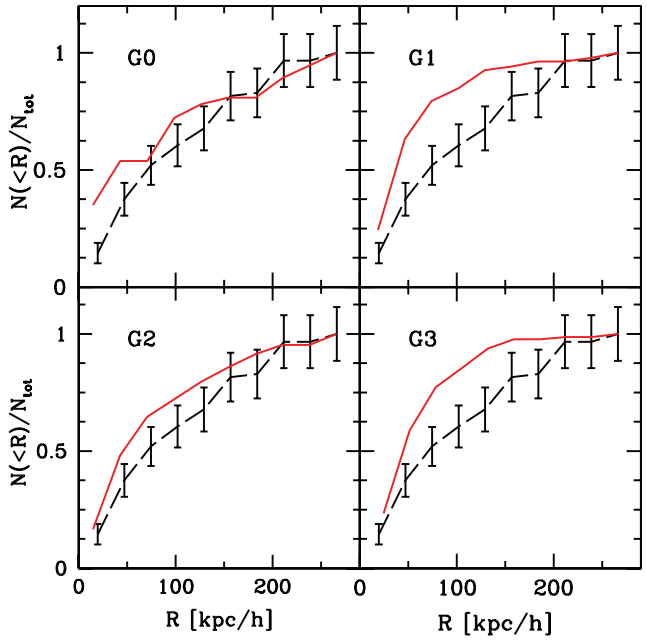

Figure 7. The fraction of satellites as a function of the distance from the central galaxy. Observational data are shown by the (black) dashed line with error bars (representing the Poisson noise). The K09 model is shown by the solid (red) line.

simply consider all satellites with $M_V < -1$ to be 'observable'). In the upper panel, we show the number density radial distribution of all 'observable' satellites ($M_V < -1$), of faint satellites ($-9 < M_V < -1$) and of classical satellites ($M_V < -9$). The number-weighted distribution of observable satellites (which are dominated by the much more numerous faint population) traces the subhalo distribution (but is down by a factor of $\sim$2) at small radii (within

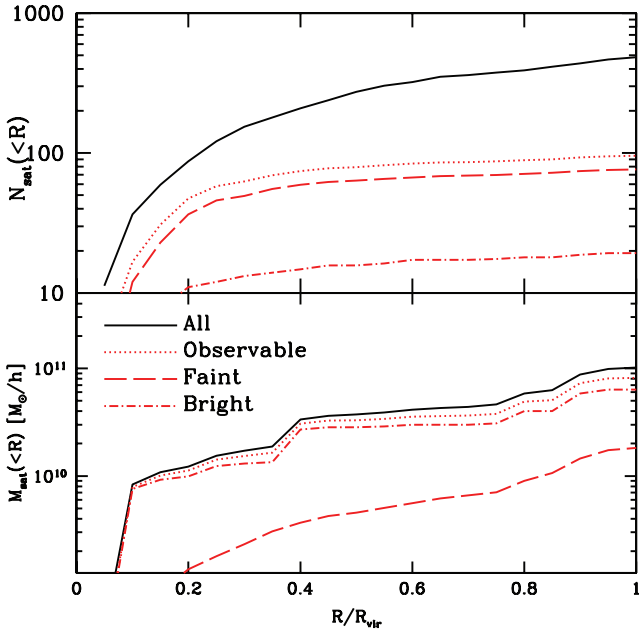

Figure 8. Upper panels: number-weighted cumulative fractional radial distribution of satellites; the black line shows all substructures (dark and observable), the (red) dotted, dashed and dot-dashed lines are for the 'observable' satellites ($M_V < -1$), the faint satellites ($-9 < M_V < -1$) and the classical satellites ($M_V < -9$), respectively. Lower panel: same as upper panels but with weighted by satellite mass. The results were obtained by averaging over the four haloes G0–G3; only the K09 model is shown.

$R/R_{\rm vir} \approx 0.2$), but flattens relative to the subhalo distribution at large radii. This implies that 'observable' subhaloes are more concentrated near the large galaxy than the overall population of subhaloes (see also Kravtsov et al. 2004). When satellites are weighted by their mass (lower panel of the same figure), the distribution is dominated by the classical (bright) satellites, and is almost identical to the mass-weighted distribution for all subhaloes. Thus, the different radial distribution of 'observable' and dark satellites is due to the suppression of star formation in low-mass haloes due to cosmic reionization and feedback processes.

5.4 Physical processes that shape the satellite LF

We have shown that it is indeed possible to reproduce the observed MW satellite LF within the ΛCDM model; we now investigate the role of various physical processes in shaping the LF in our theoretical models, with a focus on the origin of the newly discovered ultra-faint satellite population. There are several possible physical origins for the ultra-faint satellite population: it can originate from (i) object that formed in haloes with $T < 10^4$ K via H_2 cooling (e.g. Salvadori & Ferrara 2009); (ii) haloes with $T > 10^4$ K that were inefficient at accreting (hot) gas because of photoionization; (iii) haloes with $T > 10^4$ K in which star formation was inefficient because of strong SN feedback; (iv) objects that originally had larger stellar masses but have experienced significant stellar stripping.

In the following sections, we will investigate scenarios (ii)–(iv). The first scenario, in which the ultra-faint dwarfs form via H_2 cooling in haloes with $T < 10^4$ K, is not accounted for in our models. It is likely however that some ultra-faint satellites could form in this way, and this could help in explaining the small gap between the theoretical predictions and observations for $M_V \gtrsim -3$ (e.g. Fig. 4).

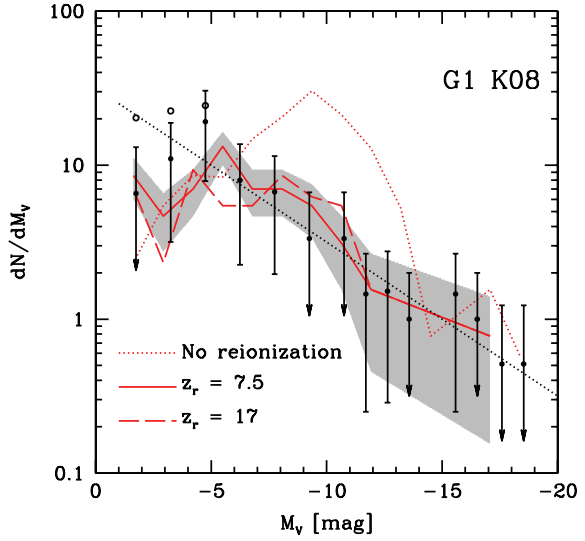

Figure 9. Satellite LF of the G1 halo in the K09 model for three different reionization redshifts. The solid line represents our fiducial model with $z_r = 7.5$, the dashed line is for $z_r = 17$, and the dotted line is for a model with no reionization (but including all other kinds of feedback). The shaded area represents the 1σ scatter around the mean of the $z_r = 7.5$ model.

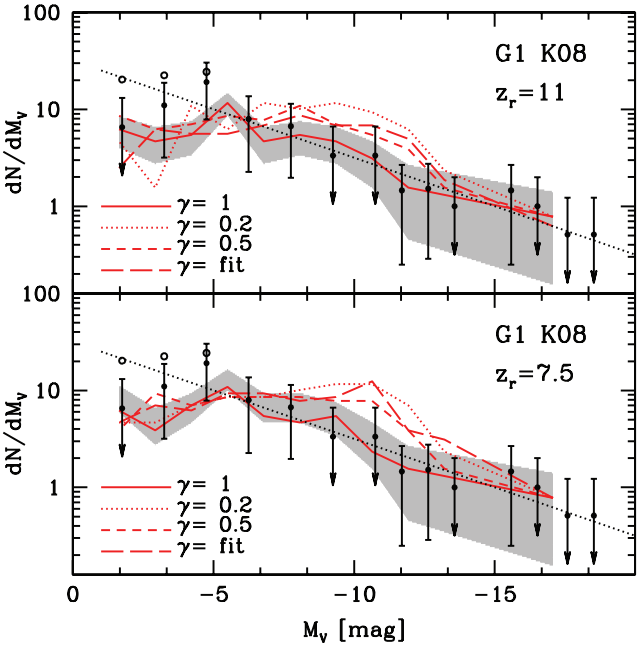

Figure 10. Satellite LF for the G1 halo in the K09 model, for different parametrizations of cosmic reionization. The solid line shows results for the standard reionization model ($\gamma = 1$, see text for the definition of γ) based on Kravtsov et al. (2004). The dotted and short dashed lines show results for a filtering mass M_F reduced by 80 and 50 per cent, respectively. The long dashed line is for a model with a redshift dependent expression for the modification of M_F (see text for more details). The shaded area represents the 1σ scatter around the mean of the $\gamma = 1$ model. The left upper and lower panels are for $z_r = 11$ and 7.5, respectively.

5.4.1 *Reionization*

We test the effect of our adopted parametrization of cosmic reionization on our results, by both varying the reionization redshift within our reference model based on Kravtsov et al. (2004) and by applying a simple modification to this model to take into account recent results based on high-resolution hydrodynamical simulations (e.g. Hoeft et al. 2006; Okamoto, Gao & Theuns 2008).

The redshift at which reionization occurs is still quite uncertain, but it is bracketed in the range $7 < z_r < 15$ (3σ range from Komatsu et al. 2009); moreover, due to the fact that reionization proceeds in an inhomogeneous way, the actual redshift of reionization for the Local Group could substantially differ from the average reionization redshift of the Universe (Weinmann et al. 2007). Fig. 9 shows the impact of varying the reionization redshift on the G1 LF for the K09 model using the standard reionization parametrization (S08 and MORGANA show a similar trend). Without any suppression of gas accretion due to reionization, the simulated LF contains too few satellites fainter than $M_V = -5$ and too many with $M_V \sim -9$. This is because, in absence of reionization, hot gas can cool very efficiently via atomic cooling, and every halo can transform a large fraction of its gas content into stars before SN feedback shuts star formation down. When the effect of reionization is taken into account, the amount of gas available for cooling and star formation is reduced in low-mass haloes, and many galaxies are shifted from intermediate luminosities ($-15 < M_V < -6$) to low luminosities ($M_V > -6$), producing a LF that is close to a power law and is in good agreement with the data. It is also interesting to note that the LF is almost insensitive to the redshift of reionization (solid line shows results for $z_r = 7.5$, dashed line for $z_r = 17$); this is in agreement with earlier results obtained by Kravtsov et al. (2004).

In addition to uncertainty about the redshift of reionization, there is still a debate about the value of the characteristic mass, M_F, below which galaxies are strongly affected by photoionization. Okamoto et al. (2008; see also Hoeft et al. 2006), using hydrodynamical simulations, recently suggested that the actual value of M_F can be significantly lower than values previously obtained (e.g. by Gnedin 2000). In order to explore the implications of their results, we introduce a factor γ that multiplies the original value of $M_F(z)$ as derived by Gnedin (2000, see equation 1). We have used two constant values for γ, namely 0.2 and 0.5, and a redshift dependent expression $\gamma(z) = (1 + z)^{1.1}/11.8$, derived from fig. B1 of Okamoto et al. (2008). The results for these three modified models are shown in Fig. 10 for the G1 halo and for the K09 model (results from the other models are similar). We see that the reduced value of M_F has the effect of increasing the number of galaxies with $M_V \sim 10$, creating a bump in the LF, with respect to the standard case, similar to what we saw in Fig. 9 for the no reionization run (dotted line). This is true especially for strong suppression of photo-ionization as in the $\gamma = 0.2$ and $\gamma(z)$ cases. Nevertheless, it is still possible to reconcile the simulated LFs with the observational data by increasing the reionization redshift, as shown in the right-hand panel of Fig. 10, where we use $z_r = 11$.

In summary, it is interesting to note the interplay between the strength of the suppression of gas accretion due to photoionization (as reflected in the filtering mass scale) and the redshift of reionization. In our standard models, in which the suppression is relatively strong (M_F is large), we find a weak dependence of the predicted LF on the adopted value of the reionization redshift, while in models with a lower overall normalization of the filtering mass, we find a stronger dependence on the redshift of reionization.

5.4.2 *Stellar stripping and tidal destruction*

In our models, we distinguish between 'stellar stripping' and 'tidal destruction'. In the former, we track the amount of *stellar* material

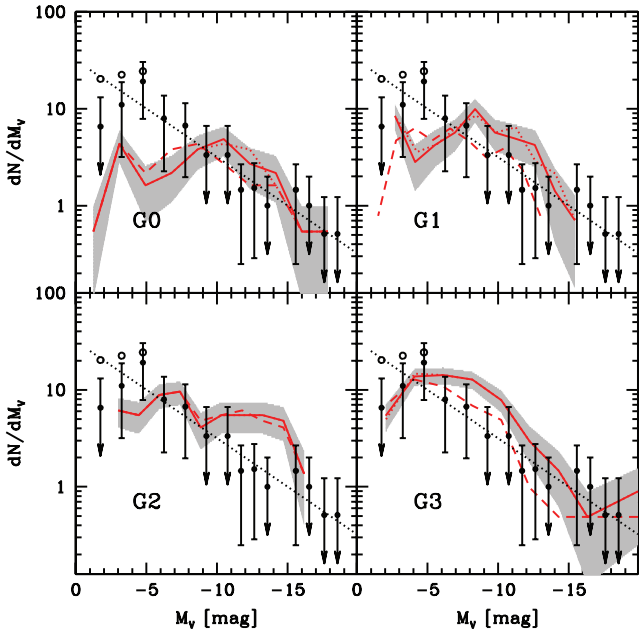

Figure 11. The effect of stellar stripping on the satellite LF. Results from the MORGANA model are shown for different levels of stellar stripping (no stripping, standard, and high). The solid line shows the moderate (standard) stripping case (as shown in Fig. 3); dotted and dashed lines show the no-stripping and strong stripping models, respectively.

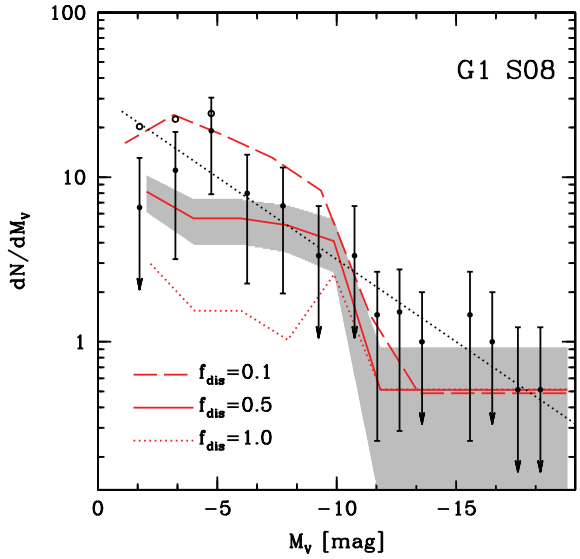

Figure 12. The effect of varying the tidal destruction parameter $f_{\rm dis}$ (see text) on the predicted MW satellite LF in the S08 model, for the G1 halo.

that is stripped from the galaxy as it orbits within the parent halo. In the latter, we assume that a satellite's baryonic mass is unaffected until its total mass is stripped by a critical amount, at which point the satellite is simply removed. Obviously, these are aspects of the same physical process and it is somewhat artificial to distinguish between them. We do so simply to illustrate the sensitivity of our results to different implementations of this physical process in models.

The MORGANA model allows for the modelling of stellar stripping as a satellite galaxy orbits around the parent galaxy (see Section 3 for more details), while the K09 and S08 models assume that the stellar content of a satellite remains unchanged until the dark matter halo is stripped beyond a certain critical point, at which point the galaxy is destroyed completely.

First, we investigate the possible effect of stellar stripping on the predicted satellite LF using the MORGANA code. We compare three different MORGANA runs with no, standard (moderate) and high stellar stripping; this latter case is obtained by increasing by a factor of 3 the fraction of stripped stellar mass with respect to the standard run (i.e. we remove from the satellites three times the mass that is beyond the tidal radius). Results for the LF are shown in Fig. 11. In the case of standard stripping the average stripped stellar mass is of the order 5–10 per cent with no mass dependence. Comparing the LF of this case with the no-stripping case, it appears that stellar stripping is almost negligible for satellites brighter that $M_V = -5$ and it marginally affects fainter satellites. When the strength of the stellar stripping is increased the mass loss is, of course, more important and as much as 40 per cent of the stellar mass can be stripped, with a strong dependence on the orbital parameters. However, even in this case the overall effect on the LF is relatively small. According to these results, stellar stripping is not one of the most important processes that shapes the satellite LF or produces ultra-faint satellites.

On the other hand, we find that the modelling of tidal destruction of satellites does have a significant effect on the satellite LF. If we neglect tidal destruction, we find many more low-mass subhaloes than are seen in the *N*-body simulations, and we would also predict many more faint satellites than are observed in the MW. Following Zentner & Bullock (2003) and Taylor & Babul (2004), the S08 model considers a satellite to be tidally destroyed when the mass of the dark matter subhalo has been stripped to a value less than or equal to the mass within $f_{\rm dis} r_{\rm s}$, where $r_{\rm s}$ is the halo's original NFW scale radius. Zentner & Bullock (2003) adopt $f_{\rm dis} = 1$ while Taylor & Babul (2004) adopt $f_{\rm dis} = 0.1$. Fig. 12 shows the effect of varying the parameter $f_{\rm dis}$ in the S08 model; we see that this can change the number of faint satellites by as much as a factor of 10. We find good agreement with the observed MW satellite LF for $f_{\rm dis} \sim 0.1$–0.5.

5.4.3 *Supernova feedback*

Feedback from SNe is believed to be an important mechanism for regulating star formation in low-mass galaxies, and it plays a primary role in shaping the LF in SAMs. It is then important to disentangle its effect from the effect of cosmic reionization discussed in the previous section. To investigate this, we first compare our reference model with both cosmic reionization and SN feedback, and a run with only cosmic reionization (no SN feedback). The results for the K09 model are shown in Fig. 13; the S08 model shows similar behaviour. In the absence of stellar feedback, the SAM predicts a deficit of faint satellites ($M_V > -5$) and an overabundance of intermediate luminosity satellites ($-15 < M_V < -10$) when compared with the observations. The inclusion of SN-driven outflows again moves intermediate luminosity galaxies into the ultra-faint regime by removing a significant fraction of the gas and thereby suppressing star formation.

As we already discussed in Section 3 the original version of the MORGANA model, implementing a recipe for SN feedback derived from Monaco (2004), does not produce good agreement with the MW satellite LF. In order to reproduce the observed MW satellite LF, we found it necessary to modify the stellar feedback modelling using an approach similar to K09 and S08.

We conclude that strongly *differential* SN feedback (in which the outflow rate relative to the star formation rate is much higher in

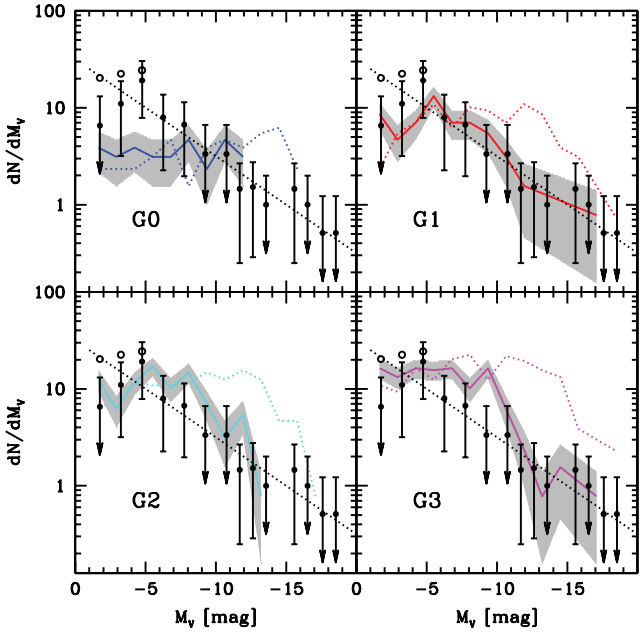

Figure 13. The effect of SN feedback on the satellite LF. Results from the K09 model with SN feedback switched *on* (solid line with shaded area) and *off* (dotted line) are shown.

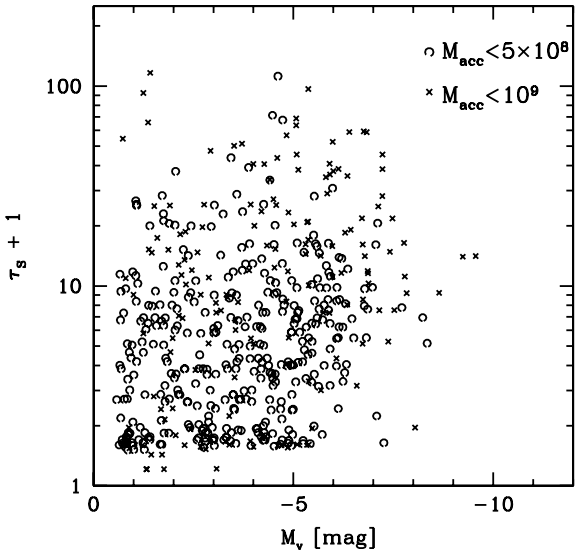

Figure 14. Relation between satellite luminosity and τ_S (defined according to equation 4) for the K09 model. Different symbols show different values for the total mass of the satellite at the time of accretion, as indicated in the figure label. Satellites with $\tau_S < 1$ may have been affected by 'strangulation'.

low-mass galaxies) plays a key role in reproducing the MW satellite LF in these models.

5.4.4 *Satellite strangulation*

There is another effect that in our models can cause relatively high-mass haloes ($T > 10^4$ K) to be inefficient at forming stars and thus to produce ultra-faint satellites. This effect is a result of the fairly standard assumption in SAMs of 'satellite strangulation', namely that the hot gas halo that could provide new gas to a galaxy is stripped immediately when a galaxy becomes a satellite in a larger halo. Thus, haloes that are accreted by the parent halo soon after they crossed the threshold for atomic cooling ($T > 10^4$ K) and thereafter are starved of any new gas cooling or accretion can have very low stellar masses.

In order to explore the importance of this effect, we look for a correlation between satellite luminosity and the time-scale τ_S, which we define as

$$\tau_S = \frac{t_{\rm acc} - t_{\rm form}}{t_{\rm cool}}, \quad (4)$$

where the formation time ($t_{\rm form}$) is defined as the time at which the halo reaches a virial temperature $T > 10^4$ K and can first begin to cool, $t_{\rm acc}$ is the time at which the galaxy is accreted by the parent halo and becomes a satellite, and the cooling time ($t_{\rm cool}$) is the time needed for the gas to radiate away all of its energy via atomic cooling, computed at $z = z_{\rm acc}$ (the standard definition of cooling time used in SAMs). Satellites with $\tau_S < 1$ may have been 'strangulated' before they were able to cool a significant fraction of their gas. Fig. 14 shows that some (about 15 per cent) of the faint satellites have $\tau_S < 1$ and therefore may have been impacted in part by this effect (though photoionization and SN feedback may still play a role in these objects as well).

6 DISCUSSION AND CONCLUSIONS

In the last few years, a new population of ultra-faint dwarf satellite galaxies has been discovered around our Galaxy. Given these new observational data, it is timely to revisit the long standing problem of the number of satellites around MW-like dark matter haloes as predicted in the ΛCDM scenario. We address this issue by combining high resolution *N*-body simulations with three different SAMs of galaxy formation. Four high resolution *N*-body simulations are used to create detailed merger trees that represent the assembly history of a Galactic dark matter halo. These merger trees are then used as common input for three SAMs for galaxy formation, namely the MORGANA model (Monaco et al. 2007), the Somerville et al. model (S08) and the Kang model (K09), to study the expected abundance and properties of satellite galaxies in the Local Group.

Because the SAMs do not use the explicit information about subhaloes from the *N*-body, but track subhalo evolution using semi-analytic recipes, we first compare the mass function and radial distribution of dark matter subhaloes predicted by the SAMs with the results directly obtained from the *N*-body simulations. We find that the parametrizations of subhalo merging and tidal stripping and destruction adopted by the S08 and K09 models are able to fairly accurately reproduce simulation results for the mass distribution and radial distribution of satellites.

We then test the LF of our simulated satellite population against the latest observational results for the MW satellite LF. Our models are all able to reproduce the LF down to a magnitude $M_V = -5$; at fainter magnitudes ($-5 < M_V < -1$) the K09 and S08 models also provide a good fit to the observational data, while the MORGANA model tends to underestimate the abundance of ultra-faint satellites, though the predictions are still consistent with the MW data at the 1σ level. All models seem to suggest a decrease in the satellite number density below $M_V \sim -5$, consistent with the assumption of a NFW like radial distribution for observed satellites.

We also perform the comparison between our model predictions and the observations in the 'observational plane', i.e. by applying 'visibility' criteria to the simulated satellites and comparing with

© 2009 The Authors. Journal compilation © 2009 RAS, MNRAS **402,** 1995–2008

the SDSS data without any completeness corrections applied. In this case, instead of assuming a radial distribution for the observed satellites (which could in principle depend on e.g. satellite mass or luminosity in a complex way), we make use of the predictions of our models for the joint distribution function of satellite luminosity and distance from the central galaxy. We again find good agreement, increasing the robustness of our results.

We investigated the main physical processes responsible for shaping the LF of MW satellites in our models. In the absence of cooling by molecular hydrogen, and in the absence of processes like photoionization, SN feedback or stellar stripping, the predicted satellite LF would show a peak at around $M_V \sim -14$ and a sharp drop-off at $M_V > -10$, with essentially *no* satellites fainter than $M_V \sim -8$ predicted. This drop below $M_V > -8$ is not due to limited numerical resolution, but rather to the sharp assumed cooling cut-off at $T < 10^4$ K (because of our adopted atomic cooling function). However, at temperatures just slightly above the atomic cooling cut-off, cooling becomes quite rapid and so in the absence of some kind of feedback or suppression mechanism, these haloes rapidly cool all of the available baryons and convert them into stars.

In our models, photoionization due to a cosmic reionizing background and SN feedback work together in order to reshape this highly peaked LF into the near-power law down to $M_v \sim -3$ that is implied by the recent SDSS observations. Photoionization suppresses the infall of hot gas into low-mass dark matter haloes, reducing the supply of baryons that are available for cooling and star formation, while SN feedback reheats cold gas and expels it from small haloes, again suppressing the efficiency of star formation. If we include only photoionization or only SN feedback, we find an excess of intermediate luminosity satellites and a shortage of ultra-faint satellites (see also Koposov et al. 2009). In agreement with previous works (e.g. Kravtsov et al. 2004), we find that the satellite LF in our 'standard' models depends only weakly on the assumed redshift of reionization.

We made use of results from the numerical hydrodynamic simulations of Gnedin (2000) to motivate our treatment of the suppression of gas infall due to the presence of a photoionizing background. A key parameter in this recipe is the 'filtering mass' or the halo mass below which the gas content is significantly reduced relative to the cosmic average. However, recent work by other groups (Hoeft et al. 2006; Okamoto et al. 2008) has found that the filtering mass may be considerably smaller than the results of Gnedin (2000) suggested. We investigate the implications of modifying the normalization and/or redshift dependence of the filtering mass as suggested by these works, and find that when a lower normalization of the filtering mass is adopted, the results are more sensitive to the redshift of reionization. We find that we can still reproduce the observed LF with the lower filtering mass if we adopt a higher reionization redshift ($z_r \sim 11$ instead of $z_r \sim 7.5$).

We investigate the impact of stellar stripping on the observed LF using the MORGANA model. We find that stellar stripping can only decrease the satellite stellar masses by at most about $\approx$20 per cent, and therefore probably has only a minor effect on the satellite LF. However, we find that the modelling of tidal *destruction* of satellites does have a significant effect on faint end of the predicted LF.

In this work, we have concentrated on the comparison with observations of one particular quantity, the statistical distributions of satellite luminosity, although naturally the SAMs provide predictions of many other galaxy properties (e.g. Lagos, Padilla & Cora 2009). This has been done mainly for two reasons: first because robust state of the art observational data have recently been made available for those two quantities and second because our goal was to directly address the so-called missing satellite problem and the origin of the newly discovered ultra-faint population. Other observed properties (such as metallicity, gas content, star formation history, etc.) contain complementary information on the formation mechanism of galactic satellites and more can be learned by studying in them in details (e.g. Okamoto et al. 2009). While the objects produced in our SAMs do resemble several properties of observed satellites we have decided to defer a more extensive explorations of those properties to a future work.

The SAMs that we use in this work were originally normalized to reproduce global quantities such as the field galaxy LF or gas fractions for relatively luminous galaxies ($M_V \lesssim -16$). They have not previously been extensively tested against observations of galaxies on these very small mass scales. In the case of the K09 and S08 models, we found that the *identical* model ingredients and even parameter values used in the standard versions of these SAMs (e.g. Kang et al. 2005, S08) were also able to reproduce the MW satellite LF. In the case of the MORGANA model, we found that the SN feedback recipe in the original model (Monaco et al. 2007) had to be modified in order to reproduce the faint satellite population. In either case, we have gained important insights about the physical recipes incorporated in these models and their applicability over a wide range of galaxy mass scales.

Our study confirms and expands on previous works that address the so-called missing satellite problem using SAMs and simulations. The main new contribution of our paper is the implementation of SAMs within merger trees extracted from numerical simulations with very high mass resolution (particle mass $m_{\rm p} \sim 4 \times 10^5\, h^{-1}\, {\rm M}_\odot$), in which each of our four Galaxy-sized halo simulations contains 2–4 million particles. Thus, unlike previous studies (e.g. Benson et al. 2002; Somerville 2002; Kravtsov et al. 2004) which compared only with the 'classical' satellite population $M_V = -9$, we can resolve the very small subhaloes that may host the newly detected population of ultra-faint satellites. We also have the advantage of multiple simulations, unlike studies based on the Via Lactea simulation (Diemand et al. 2007) alone. Although our results are in qualitative agreement with studies based on simpler analytic recipes for assigning baryons to dark matter (sub)haloes (e.g. Koposov et al. 2009), we showed that in our models, the MW satellite LF is shaped by a complex combination of different physical processes including tidal destruction, photoionization and SN feedback.

Our models neglect several other physical processes that have been discussed in the literature, and which may be important in shaping the properties of galaxies on these mass scales. Although we model the suppression of gas infall by a uniform cosmic radiation field after reionization, we do not account for the modification of the atomic cooling function by the radiation field, the possible photo-evaporation of gas from small haloes after reionization (Barkana & Loeb 1999) or photoionization by the nearby large galaxy (i.e. the radiation field of the MW; e.g. Weinmann et al. 2007). Perhaps most importantly, we neglect cooling via molecular hydrogen, and the associated complex and poorly understood possible positive and negative feedback effects connected with the formation and destruction of H_2 (e.g. Salvadori & Ferrara 2009; Ricotti, Gnedin & Shull 2008). The fact that our models are nevertheless able to reproduce the bulk of the ultra-faint satellite population *may* indicate that these other processes operate at second order or cancel each other out or may be simply a fortuitous coincidence. Certainly this bears further study.

A further concern is that standard SAMs are known to fail to reproduce the more detailed properties of satellites in larger mass hosts: although they correctly reproduce the *number* of satellites as a function of halo mass, several different SAM codes (including the ones considered here) have been shown to produce too large a *fraction* of red and passive satellites (e.g. Kimm et al. 2009 and references therein) compared with observations. The main cause of this difficulty is believed to be the standard assumption that the hot gas halo is immediately stripped when a satellite enters a larger host, thereby depriving satellites of any new supply of gas (see Kang & van den Bosch 2008 for a detailed discussion and possible solution). It is unclear whether this will impact our predictions for the very low-mass MW satellites – we defer this question to a future investigation.

If we accept this 'baryonic' solution of the 'missing satellite problem', other interesting implications follow. Our analysis predicts that roughly 1/5 of the total number of subhaloes with a present-day bound mass $M > 2 \times 10^7\,\mathrm{M}_\odot$ should be dark. In order to properly test this picture, a signature of the presence of these dark satellites is needed. One possibility is that they could be detected via gravitational lensing (e.g. Metcalf & Zhao 2002) since those small subhaloes will act as perturbers of the lensing signal coming from the main halo. Unfortunately, recent results based on numerical simulations have shown that perturbations in the lensing potential induced by (dark) satellites are very small and unlikely to explain the anomalous flux ratios of some multiple lensed quasi-stellar objects (Macciò & Miranda 2006; Macciò et al. 2006). Another possibility would be detection of γ-rays from dark matter annihilation, as the presence of substructure boosts the γ-ray signal by a factor of 4–15 relative to smooth galactic models (Diemand et al. 2008). Finally, a third possible opportunity to detect the presence of a significant dark population of subhaloes in the MW halo could come from the signatures of the interaction of such a population with the thin stellar streams in the MW halo (e.g. Odenkirchen et al. 2001; Johnston, Spergel & Haydn 2002; Ibata et al. 2002; Grillmair & Dionatos 2006).

In final summary, our results show that not only is there no longer a 'missing satellite problem', but that well-known and well-motivated astrophysical processes working within the ΛCDM framework *naturally* predict the form of the observed MW satellite LF over six orders of magnitude in luminosity. Indeed, it may be that convincing proof of the existence of the large predicted population of dark subhaloes via one of the methods suggested above (or one not yet discovered) is one of the last remaining major challenges for the ΛCDM paradigm.

ACKNOWLEDGMENTS

The authors are grateful to Jelte de Jong, Anna Gallazzi, Nicholas Martin, Christian Maulbetsch, Hans-Walter Rix and Frank van den Bosch for many stimulating discussions. AVM thanks A. Knebe for his help with the AHF halofinder. Numerical simulations were performed on the PIA and on PanStarrs2 clusters of the Max-Planck-Institut für Astronomie at the Rechenzentrum in Garching and on the zBox2 supercomputer at the University of Zürich. Special thanks to B. Moore, D. Potter and J. Stadel for bringing zBox2 to life. FF and SK acknowledge the Kavli Institute for Theoretical Physics in Santa Barbara for hospitality: this research was partially supported by the National Science Foundation under Grant No. NSF PHY05-51164. SK was supported by the DFG through SFB 439 and by a EARA-EST Marie Curie Visiting fellowship.

REFERENCES

Adelman-McCarthy J. K. et al., 2008, ApJS, 175, 297
Babul A., Rees M. J., 1992, MNRAS, 255, 346
Barkana R., Loeb A., 1999, ApJ, 523, 54
Baugh C. M., 2006, Rep. Progress Phys., 69, 3101
Belokurov V. et al., 2007, ApJ, 654, 897
Benson A. J., Frenk C. S., Lacey C. G., Baugh C. M., Cole S., 2002, MNRAS, 333, 177
Bertschinger E., 2001, ApJS, 137, 1
Bullock J. S., Kravtsov A. V., Weinberg D. H., 2000, ApJ, 539, 517
Diemand J., Kuhlen M., Madau P., 2007, ApJ, 667, 859
Diemand J., Kuhlen M., Madau P., Zemp M., Moore B., Potter D., Stadel J., 2008, Nat, 454, 735
Efstathiou G., 1992, MNRAS, 256, 43P
Fontanot F., De Lucia G., Monaco P., Somerville R. S., Santini P., 2009, MNRAS, 397, 1776
Gilmore G., Wilkinson M. I., Wyse R. F. G., Kleyna J. T., Koch A., Evans N. W., Grebel E. K., 2007, ApJ, 663, 948
Gnedin N. Y., 2000, ApJ, 542, 535
Grillmair C. J., Dionatos O., 2006, ApJ, 643, L17
Hoeft M., Yepes G., Gottlöber S., Springel V., 2006, MNRAS, 371, 401
Ibata R. A., Lewis G. F., Irwin M. J., Quinn T., 2002, MNRAS, 332, 915
Irwin M. J. et al., 2007, ApJ, 656, L13
Johnston K. V., Spergel D. N., Haydn C., 2002, ApJ, 570, 656
Kang X., 2009, in Andersen J., Bland-Hawthorn J., Nordström B., eds, Proc. IAU Symp. 254, The Galaxy Disc in Cosmological Context. Cambridge Univ. Press, Cambridge, p. 32 (K09)
Kang X., van den Bosch F. C., 2008, ApJ, 676, L101
Kang X., Jing Y. P., Mo H. J., Börner G., 2005, ApJ, 631, 21
Kimm T. et al., 2009, MNRAS, 394, 1131
Klypin A., Kravtsov A. V., Valenzuela O., Prada F., 1999, ApJ, 522, 82
Klypin A., Zhao H., Somerville R. S., 2002, ApJ, 573, 597
Knollmann S. R., Knebe A., 2009, ApJS, 182, 608
Komatsu E. et al., 2009, ApJS, 180, 330
Koposov S. et al., 2008, ApJ, 686, 279 (SK08)
Koposov S. E., Yoo J., Rix H.-W., Weinberg D. H., Macciò A. V., Escudé J. M., 2009, ApJ, 696, 2179
Kravtsov A. V., Gnedin O. Y., Klypin A. A., 2004, ApJ, 609, 482
Lagos C. D. P., Padilla N. D., Cora S. A., 2009, MNRAS, 397, L31
Li Y., Mo H. J., van den Bosch F. C., Lin W. P., 2007, MNRAS, 379, 689
Li Y.-S., Helmi A., De Lucia G., Stoehr F., 2009, MNRAS, 397, L87
Lo Faro B., Monaco P., Vanzella E., Fontanot F., Silva L., Cristiani S., 2009, MNRAS, 1225
Macciò A. V., Miranda M., 2006, MNRAS, 368, 599
Macciò A. V., Moore B., Stadel J., Diemand J., 2006, MNRAS, 366, 1529
Macciò A. V., Dutton A. A., van den Bosch F. C., Moore B., Potter D., Stadel J., 2007, MNRAS, 378, 55
Macciò A. V., Dutton A. A., van den Bosch F. C., 2008, MNRAS, 391, 1940
McConnachie A. W. et al., 2008, ApJ, 688, 1009
Macciò A. V., Kang X., Moore B., 2009, ApJ, 692, L109
Madau P., Kuhlen M., Diemand J., Moore B., Zemp M., Potter D., Stadel J., 2008, ApJ, 689, L41
Mainini R., Macciò A. V., Bonometto S. A., Klypin A., 2003, ApJ, 599, 24
Martin N. F., Ibata R. A., Chapman S. C., Irwin M., Lewis G. F., 2007, MNRAS, 380, 281
Martin N. F., de Jong J. T. A., Rix H.-W., 2008, ApJ, 684, 1075 (MdJR08)
Mateo M. L., 1998, ARA&A, 36, 435
Metcalf R. B., Zhao H., 2002, ApJ, 567, L5
Metz M., Kroupa P., Jerjen H., 2007, MNRAS, 374, 1125
Monaco P., 2004, MNRAS, 352, 181
Monaco P., Theuns T., Taffoni G., 2002, MNRAS, 331, 587
Monaco P., Fontanot F., Taffoni G., 2007, MNRAS, 375, 1189
Moore B., Ghigna S., Governato F., Lake G., Quinn T., Stadel J., Tozzi P., 1999, ApJ, 524, L19
Navarro J. F., Frenk C. S., White S. D. M., 1997, ApJ, 490, 493
Odenkirchen M. et al., 2001, ApJ, 548, L165

© 2009 The Authors. Journal compilation © 2009 RAS, MNRAS **402,** 1995–2008

Okamoto T., Frenk C. S., Jenkins A., Theuns T., 2009, preprint (arXiv:0909.0265)
Okamoto T., Gao L., Theuns T., 2008, MNRAS, 390, 920
Parkinson H., Cole S., Helly J., 2008, MNRAS, 383, 557
Peñarrubia J., McConnachie A. W., Navarro J. F., 2008, ApJ, 672, 904
Press W. H., Teukolsky S. A., Vetterling W. T., Flannery B. P., 1992, Numerical Recipes in C: The Art of Scientific Computing, 2nd edn. Cambridge Univ. Press, Cambridge
Quinn T., Katz N., Efstathiou G., 1996, MNRAS, 278, L49
Read J. I., Pontzen A. P., Viel M., 2006, MNRAS, 371, 885
Ricotti M., Gnedin N. Y., Shull J. M., 2002, ApJ, 575, 49
Ricotti M., Gnedin N. Y., Shull J. M., 2008, ApJ, 685, 21
Salvadori S., Ferrara A., 2009, MNRAS, 395, L6
Simon J. D., Geha M., 2007, ApJ, 670, 313
Somerville R. S., 2002, ApJ, 572, L23
Somerville R. S., Kolatt T. S., 1999, MNRAS, 305, 1
Somerville R. S., Primack J. R., 1999, MNRAS, 310, 1087
Somerville R. S., Primack J. R., Faber S. M., 2001, MNRAS, 320, 504
Somerville R. S., Hopkins P. F., Cox T. J., Robertson B. E., Hernquist L., 2008, MNRAS, 391, 481 (S08)
Stadel J. G., 2001, Ph.D. Thesis, Univ. Washington
Strigari L. E., Bullock J. S., Kaplinghat M., Diemand J., Kuhlen M., Madau P., 2007, ApJ, 669, 676
Strigari L. E., Bullock J. S., Kaplinghat M., Simon J. D., Geha M., Willman B., Walker M. G., 2008, Nat, 454, 1096
Taylor J. E., Babul A., 2004, MNRAS, 348, 811
Thoul A. A., Weinberg D. H., 1996, ApJ, 465, 608
Tollerud E. J., Bullock J. S., Strigari L. E., Willman B., 2008, ApJ, 688, 277
Walsh S. M., Willman B., Jerjen H., 2009, AJ, 137, 450
Wechsler R. H., Bullock J. S., Primack J. R., Kravtsov A. V., Dekel A., 2002, ApJ, 568, 52
Weinmann S. M., Macciò A. V., Iliev I. T., Mellema G., Moore B., 2007, MNRAS, 381, 367
Willman B. et al., 2005, ApJ, 626, L85
Zentner A. R., Bullock J. S., 2003, ApJ, 598, 49
Zentner A. R., Berlind A. A., Bullock J. S., Kravtsov A. V., Wechsler R. H., 2005, ApJ, 624, 505
Zucker D. B. et al., 2006, ApJ, 643, L103

This paper has been typeset from a TEX/LATEX file prepared by the author.